ACS APPLIED ELECTRONIC MATERIALS

pubs.acs.org/acsaelm Article

# Electrochromic Properties of Perovskite $NdNiO_3$ Thin Films for Smart Windows

Yifei Sun,[#] Qi Wang,[*,#] Tae Joon Park,[#] Thomas Edward Gage, Zhen Zhang, Xuejing Wang, Di Zhang, Xing Sun, Jiazhi He, Hua Zhou, Daw Gen Lim, Chengzi Huang, Haoming Yu, Xuegang Chen, Haiyan Wang, Jianguo Mei, Eric Deguns, and Shriram Ramanathan[*]

Cite This: https://doi.org/10.1021/acsaelm.1c00030 Read Online

ACCESS | Metrics & More | Article Recommendations | Supporting Information

**ABSTRACT:** Semiconductors with electrically tunable band gaps are of great interest in controlling transparency to electromagnetic radiation. Thin films of perovskite nickelate $NdNiO_3$ (NNO), a class of correlated oxides, were deposited on single-crystal ($LaAlO_3$ (LAO)) and polycrystalline (fluorine-doped tin oxide-coated glass (FTO)) substrates by magnetron sputtering, chemical solution deposition (CSD), and atomic layer deposition (ALD). Their electrochromic behaviors were investigated using a three-electrode setup in basic (KOH solution, pH = 12) electrolyte. During bleaching/coloration process, the proton intercalation/deintercalation and simultaneous electron compensation in the NNO lattice under electrical bias led to crossover of the material between the pristine-conducting phase ($Ni^{3+}$) and the strongly correlated insulating phase ($Ni^{2+}$), which serves as the working principle for electrochromic (tunable opacity in the visible range) behavior. Cyclic voltammetry (CV) scans demonstrate that NNO films are electrochemically stable in basic solutions for all three film deposition methods explored here. CV scans at varying rates enabled the extraction of diffusion coefficient of protons in thin film NNO, which is $\sim 10^{-7}$ $cm^2$ $s^{-1}$ among all films studied. Large light transmittance modulation by bleaching and coloration was observed on films grown on both LAO and FTO substrates, suggesting its potential as an electrochromic material candidate for smart windows and optical shutter applications. Porous NNO films obtained by chemical solution deposition tend to demonstrate stronger electrochromic activity than dense films grown by sputtering or ALD.

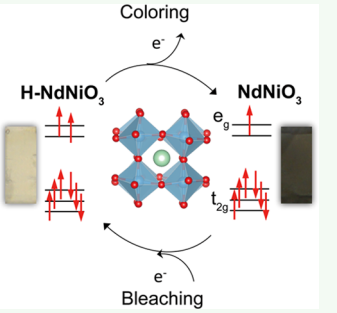


**KEYWORDS:** *electrochromic, perovskite, nickelate, thin film, strongly correlated, smart windows, tunable optics*



## INTRODUCTION

Electrochromic materials change their opacity upon application of an electrical stimulus. The change in optical properties can be nonvolatile, and the opacity level was tuned continuously by bias voltage. Such materials are actively being researched for smart windows via controlling transparency with potential applications in energy-efficient building architectures, optical shutters, and tunable optical surfaces for eye goggles, aircraft, or automotive vehicles.[1] Typical electrochromic materials operate in contact with a transparent electrolyte medium sandwiched between two electrodes. The electrolyte can be in either liquid, gel, or solid form that conducts mobile ions such as protons ($H^+$) and lithium ions ($Li^+$).[2,3] The fundamental operation principles of electrochromic inorganic oxides are based on the reversible injection of electrons and small-radius mobile cations into/out of a solid crystal lattice, accompanied by electron compensation and resulting changes in optical transparency. Time scales of interest in these diverse applications range from seconds to minutes, wherein the optical transparency modulation range is controlled by electric bias over the chosen time period.

To date, inorganic oxide materials including $WO_3$,[4] niobium oxide ($Nb_2O_5$),[5] titanium oxide ($TiO_2$),[6] nickel oxide (NiO),[7] and iridium oxide ($IrO_2$),[8] wherein the optical state can be switched between colored (e.g., blue, gray, or opaque) and transmissive, have attracted much attention owing to their diverse composition/structure, superior electrochromic performance, and stability against corrosion.[9]

The most widely studied model cathodic electrochromic system of $WO_3$ modulates its transmittance relying on the insertion of protons and charge-compensating electrons to fill into the conduction band ($t_{2g}^1$) of $WO_3$.[10] The material undergoes an insulator−metal transition accompanied by variation in electrical resistivity and optical transmittance between dark blue and transparent (Figure 1a). The electrochromic properties can vary depending on the microstructure and synthesis methods. Zhao et al. synthesized quantum dots of $WO_3$ with an average size less than 2 nm,

Received: January 11, 2021
Accepted: March 14, 2021

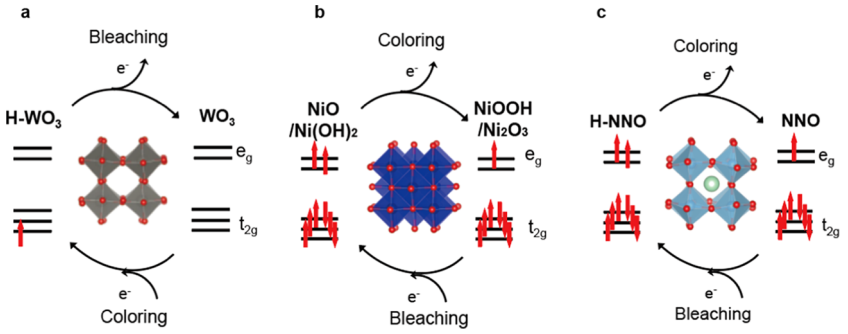


**Figure 1.** Schematic diagram of the working principle of various electrochromic materials. (a) $WO_3$ working principle. The gray and red colors represent W and O atoms, respectively. The pristine $WO_3$ is optically transmissive (bleached state) and becomes opaque after proton insertion accompanied by extra electron filling into the $t_{2g}$ orbital (colored state). (b) NiO working principle. The dark blue and red colors represent Ni and O atoms, respectively. The NiO is naturally transparent at the pristine state and colored while intercalated with extra $OH^-$ or further oxidized to $Ni_2O_3$. (c) $NdNiO_3$ working principle. The green, light blue, and red colors represent Nd, Ni, and O atoms, respectively. The nickelate is naturally opaque with single electron occupancy in the $e_g$ orbital and experiences a crossover to the double occupancy state after proton intercalation and becomes transmissive.

which showed coloration/bleaching time <1 s and a color efficiency of 154 $cm^2\ C^{-1}$.[11] Cai et al. prepared porous $WO_3$ films, which showed an ideal optical modulation capacity of 97.7% at a wavelength of 632.8 nm with switching times of 6 and 2.7 s for the coloration and bleaching, respectively.[12] Compared to the crystalline $WO_3$ film, amorphous $WO_3$ may show quicker coloration and improved efficiency. Cheng et al. reported an amorphous $WO_3$ prepared by photodeposition with an optical modulation of 70% at 700 nm and coloration efficiency >130 $cm^2\ C^{-1}$.[13] Microstructure and synthesis methods are therefore important factors in optimizing the performance of electrochromic materials and an active area of research.

In comparison, the most commonly used anodic oxide-based EC materials of Ni oxides are able to change from a transparent state to a neutral-colored one upon extraction of protons or insertion of $OH^-$ ions. Charge-balancing electrons are simultaneously extracted from the valence band to convert $Ni^{2+}$ to $Ni^{3+}$. During operation, the films are actually in the state of mixed oxide and hydroxide at the bleached state and of oxygen-rich compounds NiOOH and $Ni_2O_3$ at the colored state, which strongly absorb visible light.[14] Similarly, NiO with diverse nanostructures such as nanorods, nanosheets, and nanoflakes have been reported.[15] Ultrathin NiO nanosheet was reported to have a transmittance modulation of 40% with a coloration efficiency of 43.5 $cm^2\ C^{-1}$.[16] Patil et al. reported one-dimensional (1D) NiO nanorods with a significantly enhanced optical transmittance capability of 60%, and coloration and bleaching times of 1.55 and 1.22 s at 630 nm, respectively. Ma et al. demonstrated the synthesis of hierarchical NiO with nanoflake morphology with high optical modulation (73.2% at 550 nm) and a switching time of 1.8 s for coloration and 3.2 s for bleaching.[17]

The ionic diffusion coefficient in the switching medium places fundamental limits on operational characteristics of electrochromic materials. For example, crystalline $WO_3$ and NiO have typical proton diffusivity on the order of $10^{-8}$–$10^{-10}$ $cm^2\ s^{-1}$.[18,19] Therefore, new materials that offer comparable or improved ionic diffusion coefficient and absorption over the visible spectrum are of interest and worth exploring as potential candidates for next-generation electrochromic windows.

Rare earth nickelates with a perovskite structure ($ABO_3$) are of broad research interest due to their highly sensitive electronic phase diagram with respect to orbital electron occupancy.[20−24] As a representative, $NdNiO_3$ (NNO) shows metallic conduction behavior and is neutral gray at room temperature with single electron occupancy in the $e_g$ orbital of Ni 3d bands ($e_g^1$).[25−29] Upon cation intercalation accompanied by an extra electron filling, the Ni state in the pristine NNO experiences crossover to the $Ni^{2+}$ state that is highly localized ($e_g^2$).[30,31] The strong carrier localization opens up an optical gap and makes the material transmissive. The ion−electron intercalation therefore leads to completely opposing effects compared with $WO_3$, as shown schematically in Figure 1.

While hydrogen doping-driven changes in the conductivity of $NdNiO_3$ have been reported in the literature in the context of electronic memory device technologies,[24,26,32] properties relevant to optical window applications are still largely unknown and form the subject of this study. Here, we present experimental results on neodymium nickelate films synthesized by multiple methods (sputtering, chemical solution, and atomic layer deposition) that display promising characteristics pertaining to optical transmittance and we further compare its properties with well-studied oxide counterparts such as $WO_3$ and NiO.

## EXPERIMENTAL SECTION

**Physical Vapor Deposition (PVD) of $NdNiO_3$ Thin Films (PVD-NNO).** $NdNiO_3$ (NNO) thin films were grown on (001) $LaAlO_3$ (LAO) and fluorine-doped tin oxide (FTO, thickness 180 nm)-coated glass substrates using magnetron sputtering at room temperature combined with postannealing in air atmosphere. The deposition condition is a 40:10 sccm $Ar/O_2$ mixture at a total pressure of 5 mTorr from two metallic Ni (DC, 70 W) and Nd (RF, 170 W) targets. The deposition rate is 140 nm per hour. The as-deposited samples were annealed in air at 500 °C for 24 h in a tube furnace to form the perovskite phase. Unless specifically noted, the film thickness is ∼50 nm prepared for the characterization studies.

**Chemical Solution Deposition (CSD) of $NdNiO_3$ Thin Films (CSD-NNO).** The solution was prepared by dissolving neodymium nitrate hexahydrate ($Nd(NO_3)_3{\cdot}6H_2O$, Sigma-Aldrich, purity 99.9%) and nickel(II) acetate tetrahydrate ($Ni(CH_3COO)_2{\cdot}4H_2O$, Sigma-Aldrich, purity 99.998%) in the solvent mixture of 2-methoxyethanol and acetic acid (volume ratio 4:1), preheated at 80 °C. The solution was heated and stirred at 80 °C for 1 h and then filtered. The concentration of the solution was controlled to 0.2 M by properly weighing the two solid precursors. The spin-coating method was used to deposit NNO thin films with a spin speed of 3000 rpm and a duration of 30 s. Then, the coated films were baked at 175 °C for 20


https://doi.org/10.1021/acsaelm.1c00030
ACS Appl. Electron. Mater. XXXX, XXX, XXX−XXX

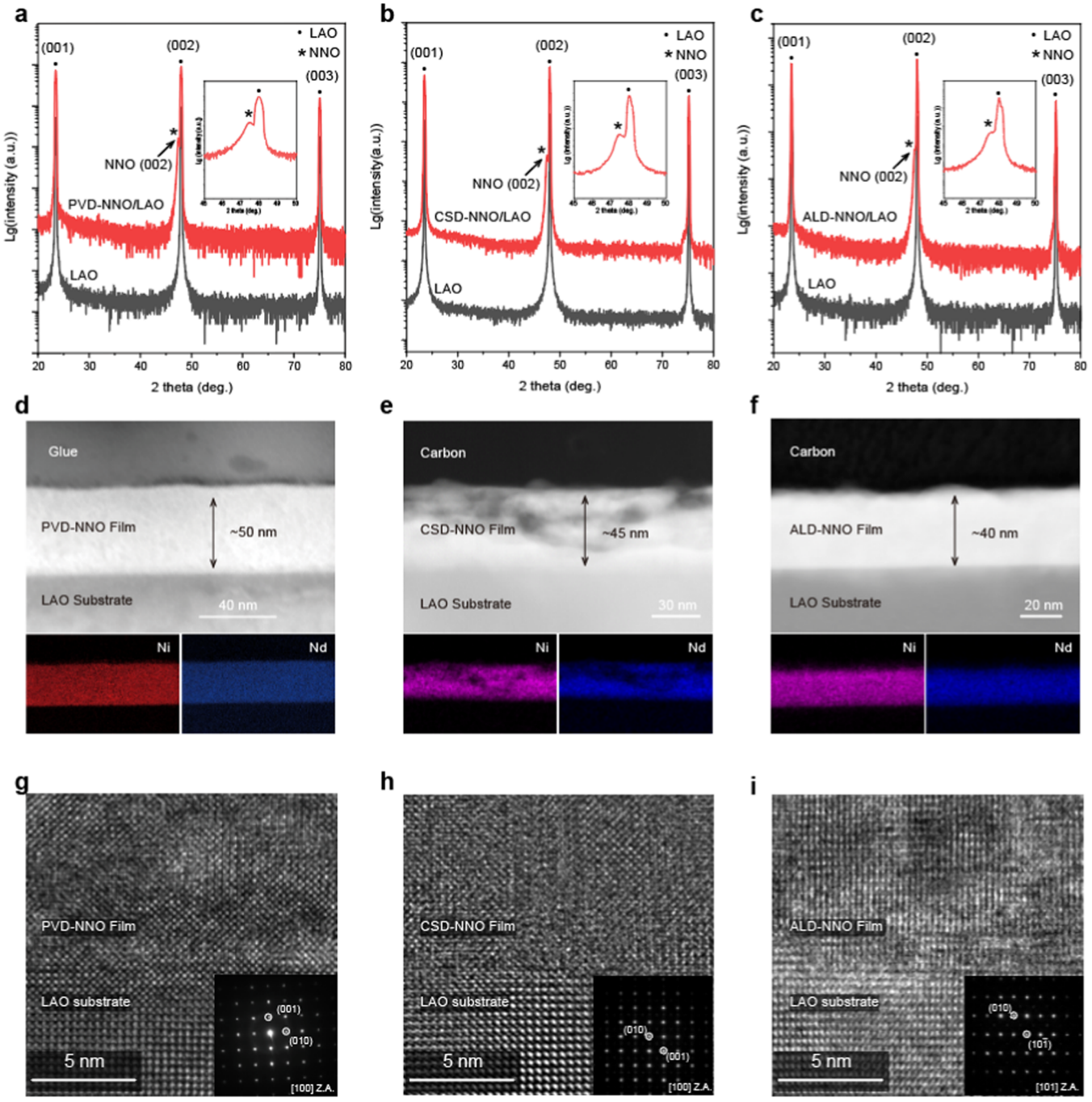


**Figure 2.** NNO thin films on the LAO substrate. (a–c) XRD scans of NNO/LAO samples deposited by PVD, CSD, and ALD. The peaks are labeled with a pseudocubic notation. The insets show the enlarged scan from 45 to 50°. NNO (002) peaks were all identified, with $2\theta_{\text{PVD-NNO}}$ at 47.47°, $2\theta_{\text{CSD-NNO}}$ at 47.48°, and $2\theta_{\text{ALD-NNO}}$ at 47.54°, which indicates that our NNO films on LAO substrates are oriented. No peaks from any secondary phases were observed. (d–f) Cross-sectional HAADF-STEM and the corresponding EDX mappings of Ni and Nd elements, which indicate a 1:1 atomic ratio in all films. The CSD-NNO/LAO thin film is porous, while the other two are dense. (g–i) High-resolution TEM images of cross-sectional NNO/LAO samples at the film/substrate interface. The selected area diffraction patterns are shown in the insets, also labeled with a pseudocubic notation.

min to evaporate any remaining solvent or water molecules. Then, the baked film was immediately transferred to the furnace for pyrolysis and annealing. The pyrolysis condition was 300 °C for 30 min in air. Subsequently, the films were annealed at 600 °C in air for 12 h.

**Atomic Layer Deposition (ALD) of $NdNiO_3$ Thin Films (ALD-NNO).** ALD depositions of $NdNiO_3$ were performed in a Veeco Savannah S200 reactor. The deposition temperature was kept at 160 °C and the pressure was 0.9 mbar, maintained by a 20 sccm of $N_2$ (Indiana Oxygen, 99.9995%). Nd(*i*PrCp)$_3$ (*i*PrCp = *i*-propylcyclopentadienyl, Strem Chemicals, 99.9%) and Ni(*t*Bu$_2$-amd)$_2$ (*t*Bu$_2$-amd = *N*,*N*-di-*t*-butylacetamidinato, Strem Chemicals, 99.999%) were used as organometallic precursors and evaporated at 160 and 125 °C, respectively, while ozone ($O_3$) with a concentration of ~200 ng mL$^{-1}$ was employed as the oxidant. Nd(*i*PrCp)$_3$ was introduced into the reactor using a "boosted" configuration, where $N_2$ was pressurized into the cylinder prior to dosing the precursor into the reactor. Ozone ($O_3$) was used as an oxygen precursor. Pulse and purge durations were 0.5/5 s for Nd(*i*PrCp)$_3$, 0.75/5 s for Ni(*t*Bu$_2$-amd)$_2$, and 0.5/5 s


https://doi.org/10.1021/acsaelm.1c00030
ACS Appl. Electron. Mater. XXXX, XXX, XXX–XXX

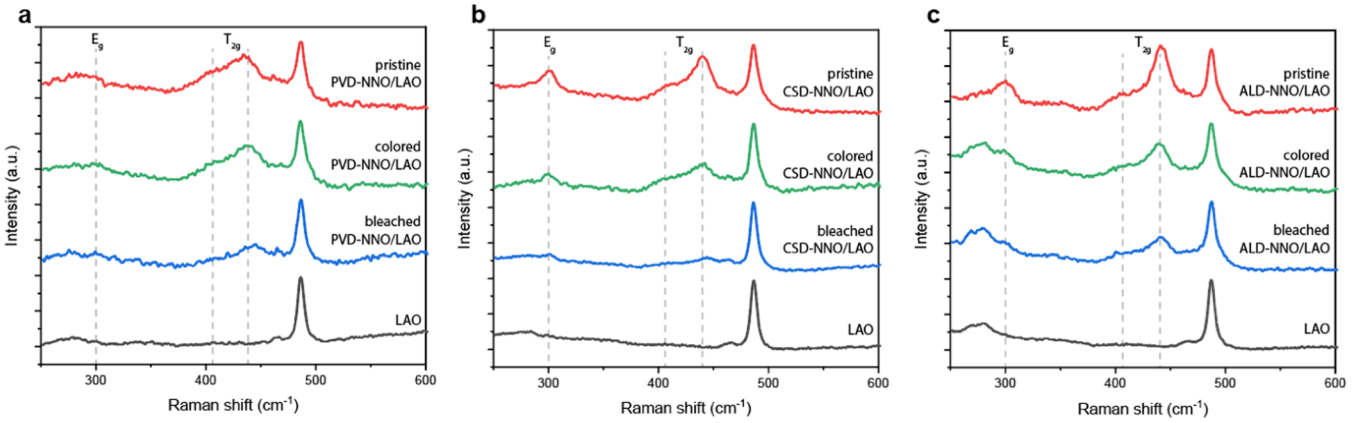


**Figure 3.** Raman spectra of NNO/LAO samples in pristine, bleached, and colored states. Vibration modes from the pristine NNO film reported in the literature are labeled by the dashed lines.[41,42] The NNO peak intensities decreased after bleaching (proton intercalation step) and partially recovered after coloration (proton deintercalation step). (a) NNO/LAO sample prepared by PVD. Bleaching condition: −0.7 V vs Ag/AgCl for 120 s. Coloration condition: +1 V vs Ag/AgCl for 180 s. (b) NNO/LAO sample prepared by CSD. Bleaching condition: −0.7 V vs Ag/AgCl for 60 s. Coloration condition: +1 V vs Ag/AgCl for 120 s. (c) NNO/LAO sample prepared by ALD. Bleaching condition: −0.7 V vs Ag/AgCl for 120 s. Coloration condition: +1 V vs Ag/AgCl for 180 s. The films at bleached and colored states were treated in a pH 12 electrolyte using a three-electrode setup.

for $O_3$. The $NdNiO_3$ films were deposited on single crystalline (001) $LaAlO_3$ (LAO) and fluorine-doped tin oxide (FTO)-coated glass substrates (MTI Corp.). All substrates were washed with toluene, acetone, and isopropanol and dried with Ar gas. After the deposition, the films were annealed at 600 °C for 24 h in air for the formation of perovskite phase. Extensive optimization experiments with precursors over a 2 year period were carried out as this is the first report on the synthesis of ALD-grown $NdNiO_3$ films. Complete details of the ALD process optimization characteristics are included in the Supporting Information.

**Electrochemical Measurements.** A basic (KOH) (0.01 M (pH = 12)) aqueous solution was utilized to study the electrochromic properties of NNO in a basic aqueous environment. A three-terminal electrochemical cell was used for both electrochromic and cyclic voltammetry (CV) measurements. A silver (Ag) wire was bonded on the thin films with silver paste. The wire contact of the electrode was covered with epoxy such that the influence of the Ag wire can be excluded. The NNO film was then submerged into aqueous solutions and denoted as a working electrode. The counter electrode was a graphite rod with a large surface area. Ag/AgCl (saturated KCl) was used as a reference electrode. For a specific cyclic voltammetry measurement, a static electric potential (vs Ag/AgCl) was applied to the NNO film by a potentiostat using a Solartron 1260A electrochemical analyzer. To obtain the diffusion coefficient of proton in the NNO film, the Randles−Sevcik (R−S) equation (i.e., $I_p/A = 268\,600\ n^{1.5}C(Dv)^{0.5}$) was used to fit the relation between the peak cathodic current density ($I_p/A$, in amps $cm^{-2}$) and the square root of scan rate ($v^{0.5}$), where $C$ is the concentration of the reaction-involved species in solution (mol $mL^{-1}$); $D$ is the diffusion coefficient of proton in NNO at room temperature ($cm^2\ s^{-1}$); $v$ is the scan rate (V $s^{-1}$); and $n$ is the number of electron exchange in the redox process between $Ni^{3+}$ and $Ni^{2+}$, which is 1.[33,34]

**X-ray Diffraction.** X-ray diffraction (XRD) patterns were collected using Panalytical MRD X'Pert Pro XRD and Bruker D8 focus XRD instruments.

**Raman Spectroscopy.** Raman spectra were collected using an inVia confocal Raman micro-spectrometer (Renishaw, U.K.), utilizing a 532 nm solid-state laser.

**Transmittance Modulation of Films.** Optical characterization was carried out using a UV−vis−NIR spectrophotometer (PerkinElmer Lambda 1050 and Lambda 950). The bare substrate (LAO- or FTO-coated glass) was used as a reference for each measurement.

**Scanning Electron Microscopy (SEM).** SEM images of the NNO films were taken by a Thermo Scientific Apreo SEM and Hitachi S-4800 field emission SEM (FE-SEM).

**Transmission Electron Microscopy (TEM).** A cross-sectional sample was lifted out of NNO samples prepared by CSD and ALD by a Zeiss 1540XB CrossBeam focused ion beam FE-SEM system. Using a Gatan precision ion polishing system (PIPS) II, these samples were further thinned down to less than 100 nm. The cross-sectional sample of PVD-NNO was prepared by conventional polishing. High-angle annular dark-field scanning transmission electron microscope (HAADF-STEM) imaging and X-ray energy-dispersive spectroscopy (EDS) mapping were performed with an FEI Talos F200X TEM. High-resolution transmission electron microscopy (HR-TEM) characterizations on representative samples grown by PVD were performed by an FEI Talos F200X TEM operated at 200 kV, while the films grown by CSD and ALD were characterized using the Argonne chromatic aberration-corrected TEM (an FEI Titan 80-300 ST with an image aberration corrector to correct both spherical and chromatic aberrations) at an accelerating voltage of 200 kV.

## RESULTS

**Electrochromic Behavior of PVD-NNO, CSD-NNO, and ALD-NNO.** NNO thin films with a nominal thickness of 40−50 nm were deposited onto single-crystal $LaAlO_3$ (LAO) substrates by PVD, CSD, and ALD, respectively. Figure 2a−c shows $\theta$−$2\theta$ XRD patterns of NNO grown on LAO substrates, and the insets show the enlarged patterns at $2\theta$ = 45−50°. The diffraction pattern indicates that the growth of the NNO film deposited by each method is highly [001]-oriented ($2\theta_{LAO}$ at 47.98°, $2\theta_{PVD\text{-}NNO}$ at 47.47°, $2\theta_{CSD\text{-}NNO}$ at 47.48°, and $2\theta_{ALD\text{-}NNO}$ at 47.54°) without any contribution from secondary phases.[35] Such an epitaxial relation can be understood based on the close matching of the pseudocubic unit cell parameter of NNO ($a_{NNO}$ = 3.81 Å) with the cubic unit cell parameter of LAO ($a_{LAO}$ = 3.789 Å) and has been noted in the literature.[36]

The morphology of representative epitaxial NNO/LAO films was analyzed by transmission electron microscopy (TEM) and is shown in Figure 2d−i. The high-angle annular dark-field (HAADF-STEM) image and energy-dispersive X-ray (EDX) mapping (Figure 2d−f) results demonstrate the uniform dispersion of Nd and Ni, and the estimated atomic ratio is ∼1 across the film thickness for the three films. Compared with PVD-NNO/LAO and ALD-NNO/LAO, the CSD-NNO/LAO film was relatively porous due to the nature of solution deposition followed by high-temperature anneal-


https://doi.org/10.1021/acsaelm.1c00030
ACS Appl. Electron. Mater. XXXX, XXX, XXX−XXX

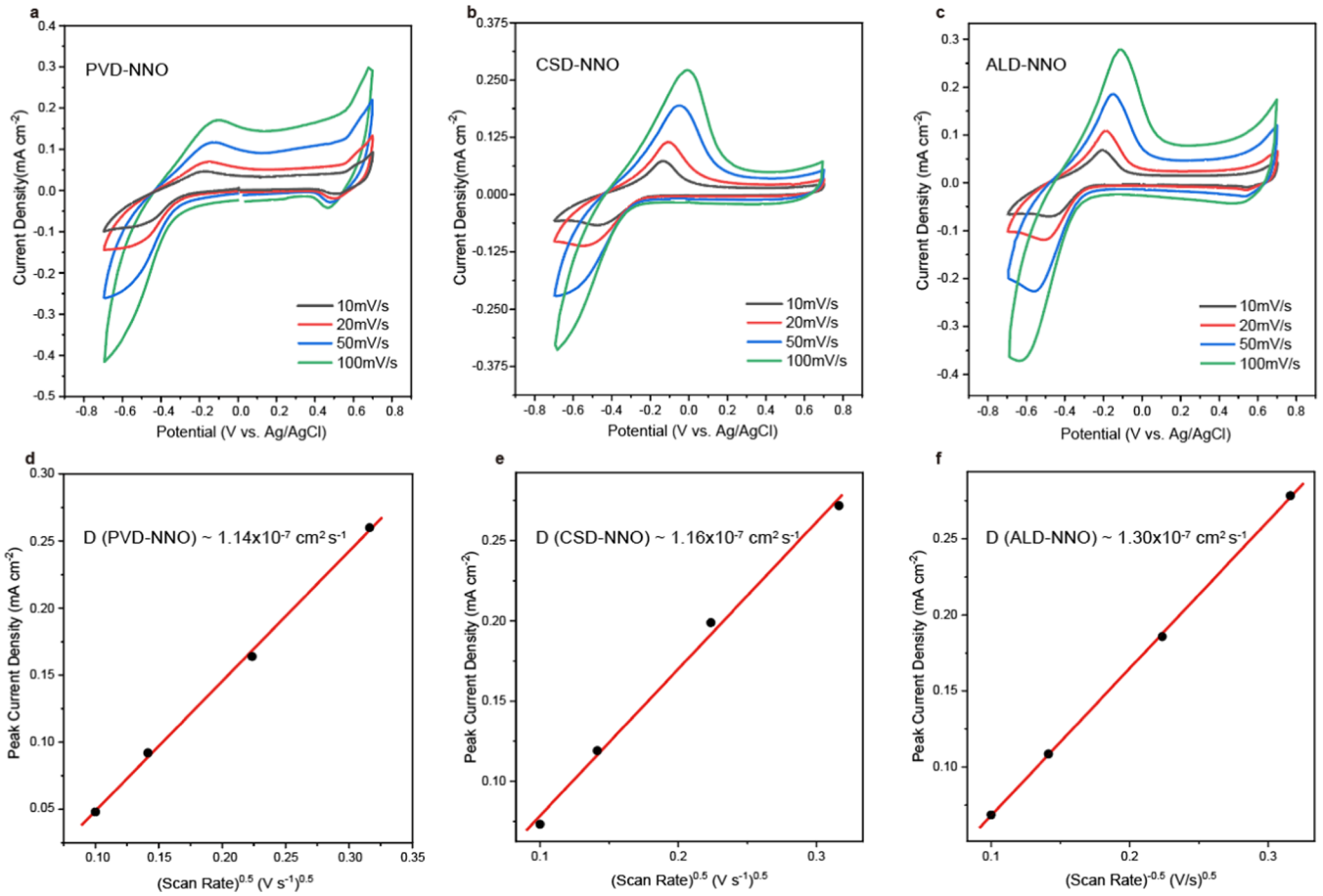


**Figure 4.** CV scans at various scan rates and the corresponding proton diffusion coefficients in NNO/LAO films. NNO films deposited by (a) PVD, (b) CSD, and (c) ALD on the LAO substrate were scanned by the CV technique at 10, 20, 50, and 100 mV $s^{-1}$ in a pH 12 electrolyte. (d–f) Linear fittings between the peak anodic current density ($I_p/A$) and the square root of the CV scan rate ($\nu^{0.5}$) were used to extract the proton diffusion coefficient in films, $D$, which are noted in the plots. In all cases, the proton diffusion coefficient was extracted to be in the similar range of ~$10^{-7}$ $cm^2$ $s^{-1}$.

ing.[37−40] Cross-sectional high-resolution TEM images of NNO/LAO films are shown in Figure 2g–i, suggesting the oriented growth of NNO by all three deposition methods.

Raman spectra evolution of NNO/LAO films before and after the proton uptake is shown in Figure 3. The Raman peaks of the LAO substrate between 450 and 550 $cm^{-1}$ could be identified in all spectra. Generally, the distorted perovskite nickelate exhibits 24 Raman-active modes, but only a few of them can be detected in the experiment.[41] The pristine NNO films show the expected peaks at ~300 $cm^{-1}$ ($E_g$ mode), ~410 $cm^{-1}$ ($T_{2g}$ mode), and ~438 $cm^{-1}$ ($T_{2g}$ mode), which is consistent among all three samples.[41,42] All peak intensities from NNO, especially the $T_{2g}$ peak at ~438 $cm^{-1}$, strongly decreased after the films were bleached in the basic electrolyte and later partially recovered after coloration treatment. The bleaching conditions for PVD-NNO/LAO and ALD-NNO/LAO samples were −0.7 V vs Ag/AgCl for 120 s, while for CSD-NNO/LAO, it was −0.7 V vs Ag/AgCl for 60 s. The coloration conditions for PVD-NNO/LAO and ALD-NNO/LAO films were +1 V vs Ag/AgCl for 180 s and +1 V vs Ag/AgCl for 120 s for the CSD-NNO/LAO sample.

Cyclic voltammetry (CV) scans were performed by a three-electrode electrochemical cell consisting of a working electrode (NNO films), a counter electrode (graphite rod), and a reference electrode (Ag/AgCl). The CVs were measured on NNO/LAO films in a 0.01 M KOH (pH = 12) electrolyte with a linear potential sweep at various scan rates ranging from 100 to 10 mV $s^{-1}$ to identify the insertion/extraction process of protons with a visible color change. Pairs of redox peaks (at −0.6/−0.1 V) can be observed on all three NNO/LAO films during the charge/discharge process, which indicates that the capacity behavior in CV measurement is due to faradic redox reactions between $Ni^{3+}$ and $Ni^{2+}$. The electrochromic phenomena of NNO in a 0.01 M KOH solution could be described as follows

$$NdNiO_3\ (\text{opaque}) + H_2O + e^- \underset{\text{coloration}}{\overset{\text{bleaching}}{\rightleftharpoons}} H - NdNiO_3\ (\text{transparent}) + OH^-$$

During CV measurements, specifically, the anodic current peaks at high potentials corresponding to the charge transfer as the $Ni^{2+}$ is oxidized. This peak shifted to low-potential regime as the scan rate decreased, indicating that the reaction is kinetically limited by the charge and mass transfer. Figure 4d–f shows the linear fitting between the maximum peak anodic current density ($I_p/A$) and the square root of the scan rate ($\nu^{0.5}$) by using the R–S equation.[33] Based on the extrapolated slopes, the estimated proton diffusion coefficients of PVD-NNO/LAO, CSD-NNO/LAO, and ALD-NNO/LAO were 1.14 × $10^{-7}$, 1.16 × $10^{-7}$, and 1.30 × $10^{-7}$ $cm^2$ $s^{-1}$,


https://doi.org/10.1021/acsaelm.1c00030
ACS Appl. Electron. Mater. XXXX, XXX, XXX−XXX

**Table I. Diffusion Coefficient of Protons in Representative Electrochromic Oxides**

| materials | electrolyte | R.T. proton diffusion coefficient ($cm^2\ s^{-1}$)[a] | calculation method | preparation method | references |
|---|---|---|---|---|---|
| polycrystalline $WO_3$ | 1 N $H_2SO_4$ | $4 \times 10^{-8}$ | R−S equation | evaporation | 44 |
| crystalline $WO_3$ | poly-AMPS[b] | $2 \times 10^{-11}$ | AC impedance | evaporation | 43 |
| amorphous $WO_3$ | poly-AMPS[b] | $4 \times 10^{-10}$ | AC impedance | evaporation | 43 |
| amorphous $WO_3$ | water-based electrolyte | $2.5 \times 10^{-7}$–$2.5 \times 10^{-9}$ | N/A | N/A | 59 |
| amorphous $WO_3$ | organic molecules | $\leq 2.5 \times 10^{-13}$ | Fick's law | N/A | 19 |
| crystalline $WO_3$ | organic molecules | $\geq 2.5 \times 10^{-7}$ | Fick's law | N/A | 19 |
| $Ni_{1-x}V_xO_y$ | 1 M KOH | $2.5 \times 10^{-16}$ | R−S equation | sputtering | 18 |
| NiOH | 1 M $HClO_4$ | $4.0 \times 10^{-11}$ | finite diffusion model | commercial | 45 |
| $MoO_3$ | 1 M $H_2SO_4$ | $1.55 \times 10^{-10}$ | R−S equation | CVD | 60 |
| $TiO_2$ | 1 M $(NH_4)_2SO_4$ | $2 \times 10^{-11}$ | R−S equation | PVD | 61 |
| NNO grown by PVD | pH = 12 KOH | $1.14 \times 10^{-7}$ | R−S equation | PVD | this work |
| NNO grown by CSD | pH = 12 KOH | $1.16 \times 10^{-7}$ | R−S equation | CSD | this work |
| NNO grown by ALD | pH = 12 KOH | $1.30 \times 10^{-7}$ | R−S equation | ALD | this work |

[a]R.T.: room temperature. [b]Polymerized 2-acrylamido-2-methylpropane sulfonic acid.

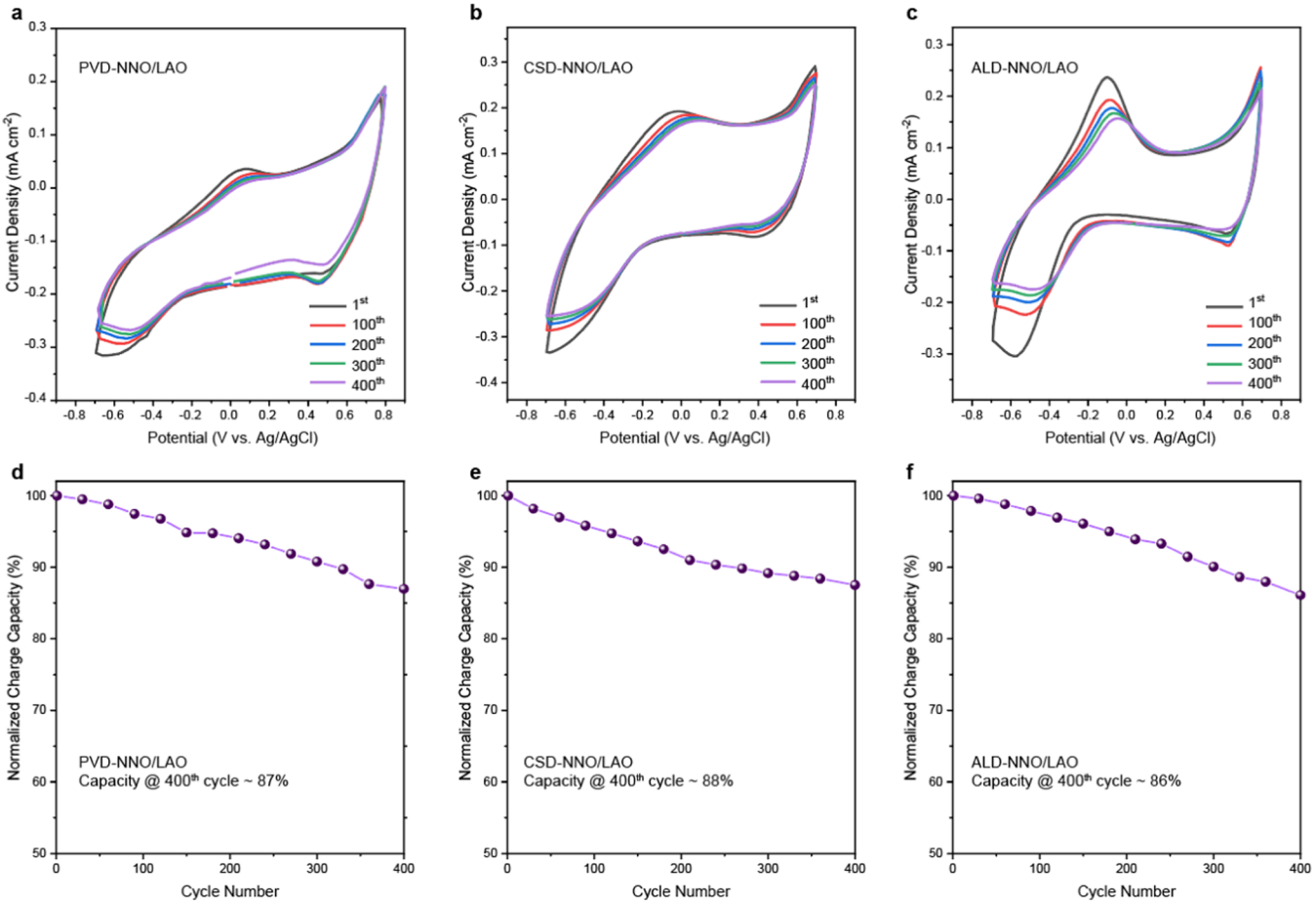


**Figure 5.** Electrochemical stability of various NNO/LAO samples in a pH 12 electrolyte. (a) PVD-NNO/LAO, (b) CSD-NNO/LAO, and (c) ALD-NNO/LAO were examined by CV scans with a scan rate of 100 mV $s^{-1}$ for 400 cycles. The initial charge capacity after 400 CV cycles for (d) PVD-NNO/LAO, (e) CSD-NNO/LAO, and (f) ALD-NNO/LAO was ~87, 88, and 86%, respectively, which indicates that the NNO/LAO samples are quite stable in basic solutions.

respectively. A comparison of the proton diffusion coefficient with other electrochromic metal oxides is shown in Table I. In comparison, the proton diffusion coefficients for $WO_3$ ranging between $10^{-7}$ and $10^{-13}$ $cm^2\ s^{-1}$ and for NiO ranging from $10^{-11}$ to $10^{-16}$ $cm^2\ s^{-1}$ have been reported in the literature and are both crystallinity- and electrolyte-dependent.[18,19,43−45]

The electrochemical stability of NNO films in a pH 12 environment was investigated by continuous cycling of the applied potential from −0.7 to +0.7 V (vs Ag/AgCl) at 100 mV $s^{-1}$. The change in the film electroactivity, which is represented by the charge capacity within each CV cycle, is used to evaluate the stability.[46−48] It was observed from the electrochemical stability graphs that PVD-NNO/LAO, CSD-NNO/LAO, and ALD-NNO/LAO can maintain >85% of their initial electroactivities after 400 cycles (Figure 5). This result shows that despite the choice of the deposition method,


https://doi.org/10.1021/acsaelm.1c00030
ACS Appl. Electron. Mater. XXXX, XXX, XXX−XXX

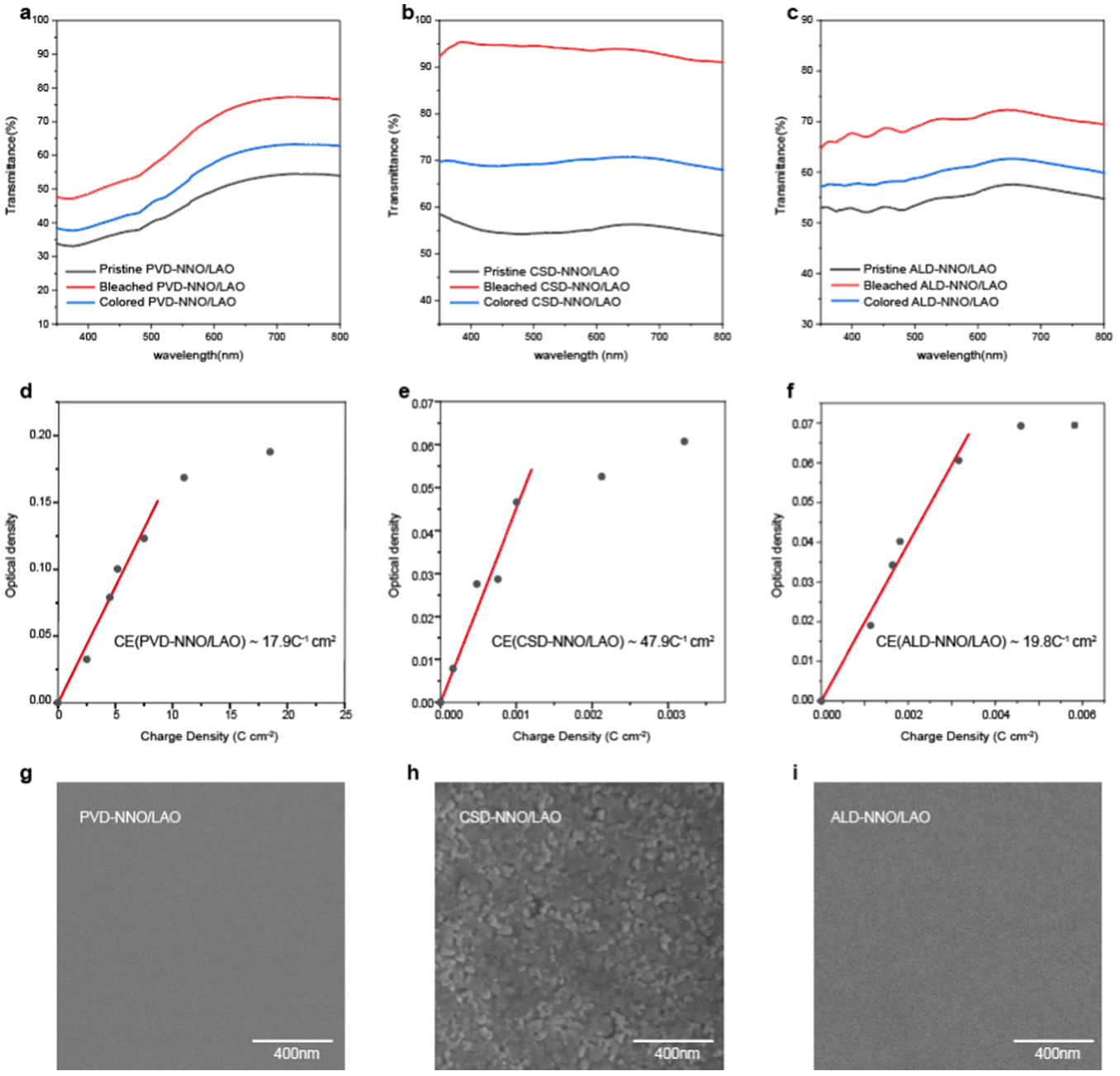


**Figure 6.** Optical transmittance modulation of ∼50 nm NNO/LAO films and the coloration efficiency. (a−c) UV−vis spectra of NNO/LAO films prepared by (a) PVD, (b) CSD, and (c) ALD in their pristine (no treatment), bleached (−0.7 V vs Ag/AgCl 30 s), and colored (+1 V vs Ag/AgCl 60 s for (a, c) and 180 s for (b) due to the dramatic transmittance increase of CSD-NNO after bleaching) states in pH = 12 electrolyte. (d−f) Coloration efficiency (CE) of NNO/LAO films prepared by (d) PVD, (e) CSD, and (f) ALD. By linear fitting, the extracted CE values are noted in each figure. The SEM images of (g) PVD-NNO/LAO and (i) ALD-NNO/LAO indicate that the films prepared by these two methods are dense, while SEM of (h) CSD-NNO/LAO shows that the film is porous and granular.

NNO/LAO films consistently show good electrochemical stability in basic solutions. This observation is similar to previous works on binary NiO.[10]

Figure 6a−c shows the optical transmittance spectra of NNO/LAO samples in their pristine (no treatment), bleached, and colored states measured in the visible wavelength range of 350−800 nm. The optical transmittance spectrum from a bare LAO substrate was used as the reference. At a wavelength of 632.8 nm, the optical transmittance modulation of NNO films is listed in Table II. The bleaching treatment (−0.7 V vs Ag/AgCl for 30 s) led to the transmittance increase of PVD-NNO/LAO, CSD-NNO/LAO, and ALD-NNO/LAO by 24, 38, and 15%, respectively. The transmittance of CSD-NNO after bleaching was higher than 90%. Further coloration treatment modulates the transmittance of PVD-NNO, CSD-NNO, and ALD-NNO films by 14, 24, and 10%, respectively. Due to the larger transmittance change in CSD-NNO after bleaching, the coloration time was slightly longer than that for PVD-NNO and ALD-NNO samples.

The coloration efficiency (CE) is defined as the change in optical density (ΔOD) per injected charge density ($Q$) at a


https://doi.org/10.1021/acsaelm.1c00030
ACS Appl. Electron. Mater. XXXX, XXX, XXX−XXX

**Table II. Optical Transmittance Modulation of NNO Films at 632.8 nm**

| materials | pristine | bleached (−0.7 V vs Ag/AgCl 30 s) | colored (+1 V vs Ag/AgCl 60 s) |
|---|---|---|---|
| 50 nm PVD-NNO/LAO | 50% | 74% | 60% |
| 50 nm CSD-NNO/LAO | 56% | 94% | 70%[a] |
| 50 nm ALD-NNO/LAO | 57% | 72% | 62% |
| 50 nm PVD-NNO/FTO glass | 48% | 75% | 58% |
| 50 nm CSD-NNO/FTO glass | 67% | 91% | 74% |
| 100 nm CSD-NNO/FTO glass | 55% | 94% | 60%[a] |
| 50 nm ALD-NNO/FTO glass | 61% | 72% | 67% |

[a]The coloration condition was +1 V vs Ag/AgCl for 180 s.

specific wavelength (632.8 nm in our case). The change in optical density is obtained from eqs 1 to 2

$$\mathrm{CE} = \frac{\Delta \mathrm{OD}(\lambda)}{Q} \tag{1}$$

$$\Delta \mathrm{OD}(\lambda) = \log\left(\frac{T_b}{T_c}\right) \tag{2}$$

where $T_c$ and $T_b$ are the transmittance in the colored and bleached states, respectively. The relationship between ΔOD and the charge density variation is shown in Figure 6d−f. CE can be estimated from the slope of the linear fitting range of the curve. This method is commonly used for studying electrochromic materials.[37,49−53] The coloration efficiency of dense films like PVD-NNO/LAO or ALD-NNO/LAO is less than 20 $cm^2\ C^{-1}$, as shown in Figure 6d,f. The coloration efficiency for CSD-NNO/LAO could reach 47.9 $cm^2\ C^{-1}$ (Figure 6e). It is close to the reported values from porous $WO_3$ and NiO (typically around 40−50 $cm^2\ C^{-1}$ [19,51,54]) and is 2−3 × the value obtained for PVD-NNO/LAO or ALD-NNO/LAO thin films. A primary reason for the difference among NNO films deposited by different methods could be the denser nature of the PVD and ALD films that limits the interfacial area between the active metal oxide grains and the protons from the electrolyte, limiting the electrochromic efficiency.[55,56] The SEM images in Figure 6g−i confirm that the CSD-NNO/LAO film has a relatively porous, granular morphology and could be suitable for further optimization of electrochromic activity.

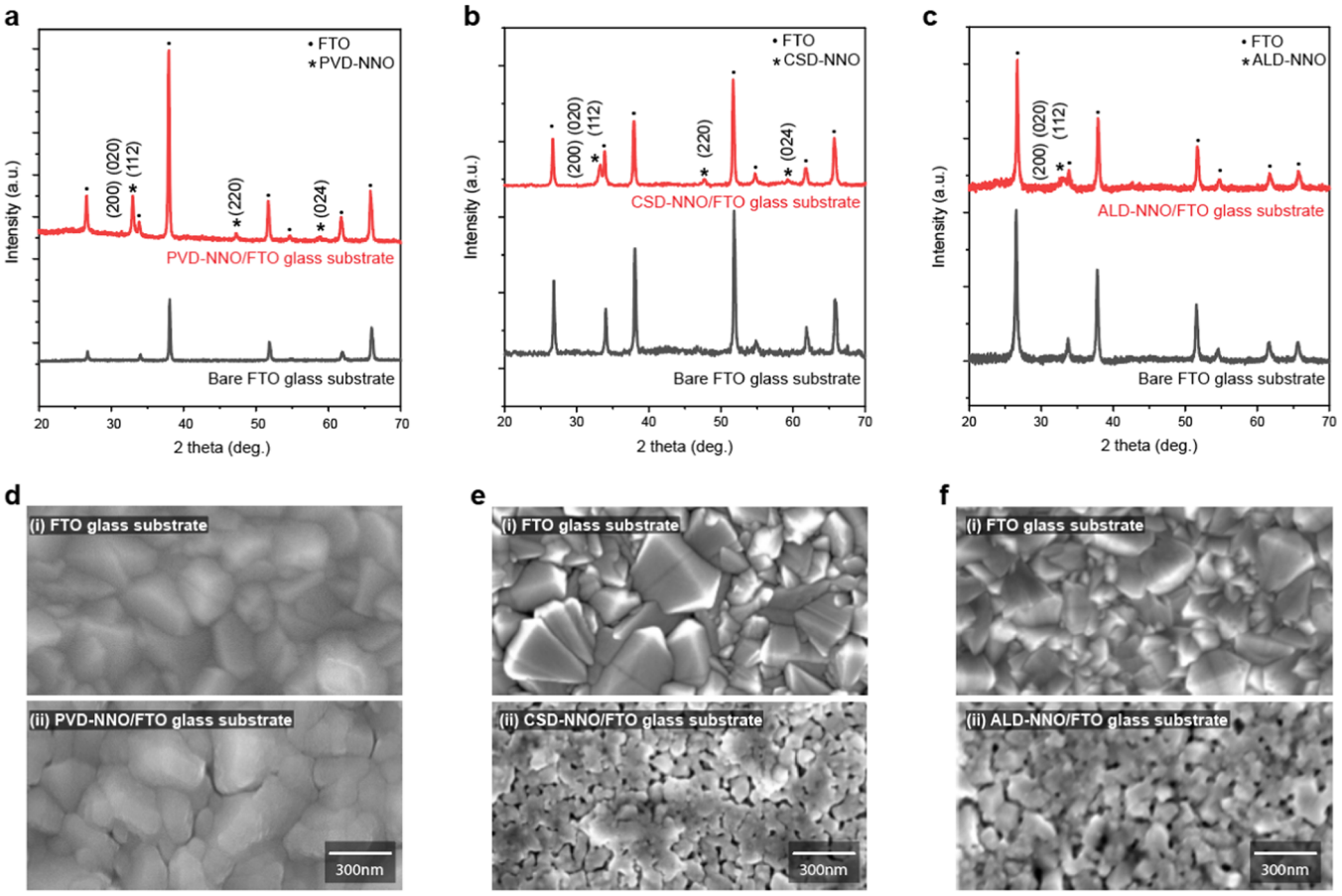


**Figure 7.** Polycrystalline NNO/FTO samples. (a−c) XRD patterns taken from ∼200 nm PVD-NNO/FTO, ∼200 nm CSD-NNO/FTO, and ∼50 nm ALD-NNO/FTO and bare FTO glass substrate reference. Only one peak was identifiable in ∼50 nm ALD-NNO/FTO due to the thinner film. (d−f) Morphology of NNO films grown on FTO along with bare FTO substrates as reference for each case. NNO film prepared by PVD (d-(ii)) or ALD (f-(ii)) tends to follow the morphology of FTO (d-(i)) and (f-(i)). The resulting polycrystalline PVD-NNO/FTO or ALD-NNO/FTO film is composed of randomly oriented small grains.


https://doi.org/10.1021/acsaelm.1c00030
ACS Appl. Electron. Mater. XXXX, XXX, XXX−XXX

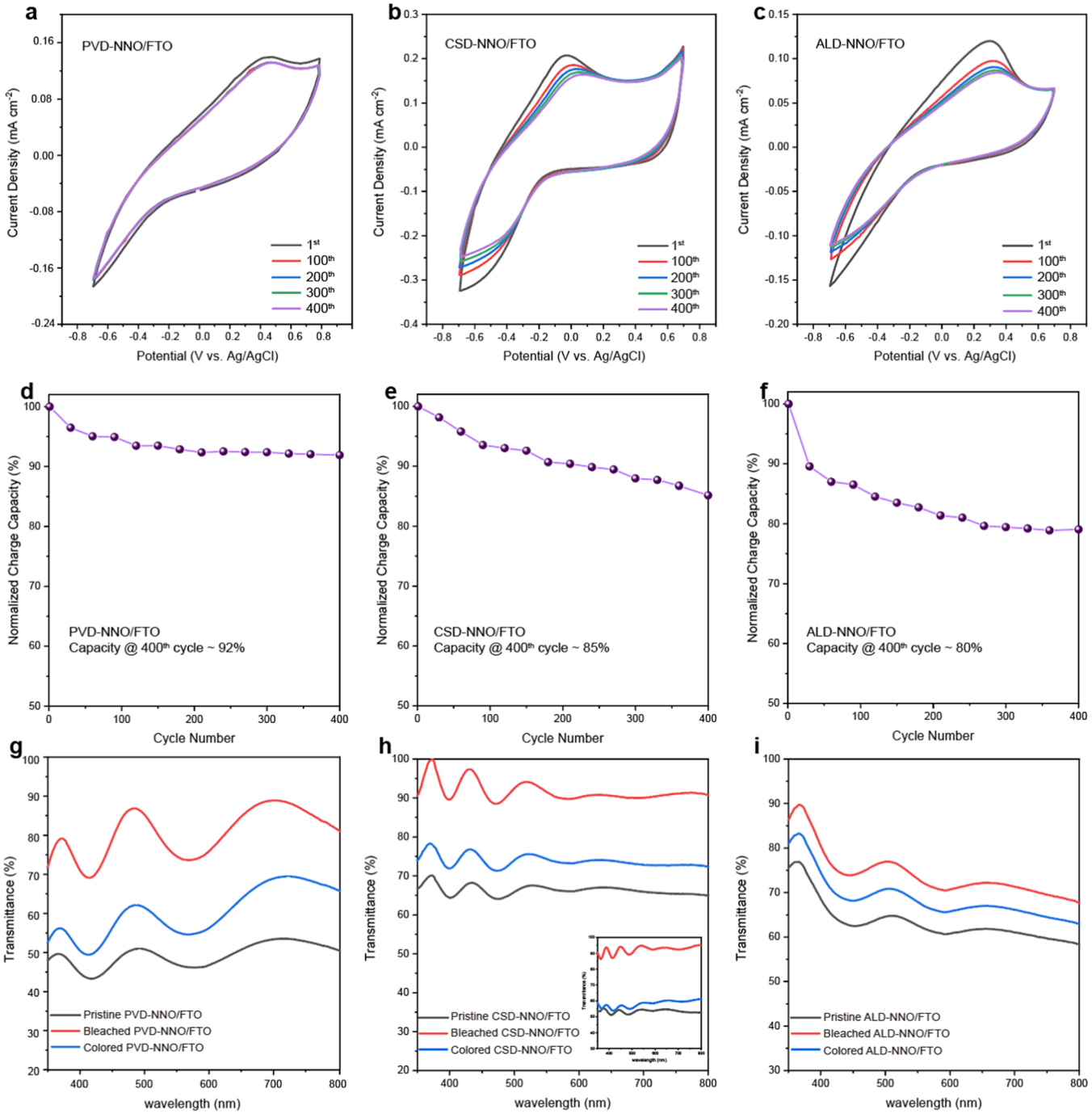


**Figure 8.** Electrochromic properties of polycrystalline NNO/FTO thin films. (a–c) CV stability test of NNO/FTO thin films in a pH 12 electrolyte. (d–f) Charge capacity maintained after 400 cycles was ~92, ~85, and ~80% for PVD-NNO/FTO, CSD-NNO/FTO, and ALD-NNO/FTO, respectively. (g–i) UV–vis spectra of pristine, bleached (−0.7 V vs Ag/AgCl for 30 s), and colored (+1 V vs Ag/AgCl for 60 s) NNO/FTO films with a thickness of ~50 nm. The inset of (h) shows the UV–vis spectra taken from a 100 nm CSD-NNO/FTO sample at pristine, bleached (−0.7 V vs Ag/AgCl for 30 s), and colored (+1 V vs Ag/AgCl for 180 s) states, which shows much better opaque/transparent contrast based on comparable pristine transmittance with 50 nm PVD-NNO/FTO (g) or 50 nm ALD-NNO/FTO (i).

We then examined the properties of NNO films grown by the above methods on the FTO-coated glass substrate for the potential smart window application. Figure 7a–c shows XRD patterns of the NNO film grown on FTO-coated glass. Besides the diffraction peaks of FTO, three XRD diffraction peaks at 33.3, 47.78, and 59.5° belonging to polycrystalline NNO were observed.[57] The electrochemical stability of NNO/FTO films was also examined by cyclic voltammetry, which confirms that polycrystalline NNO could maintain >80% of the initial activity after 400 cycles (Figure 8a–f). We noticed that the peak-to-peak separation of CVs in PVD-NNO/FTO and ALD-NNO/FTO is larger than that of corresponding NNO films grown on LAO substrates. This could be likely due to the limited diffusion as well as charge transfer in dense films deposited by PVD and ALD, as shown in Figure 7d,f. However, CSD-NNO/FTO showed a similar CV peak


https://doi.org/10.1021/acsaelm.1c00030
ACS Appl. Electron. Mater. XXXX, XXX, XXX–XXX

potential to single crystalline NNO/LAO films due to the microstructural differences as discussed in the above section. The transmittance change between colored and bleached states of NNO/FTO films is shown in Figure 8g–i. At a wavelength of 632.8 nm, the transmittance modulation of NNO/FTO samples is listed in Table II (transmittance of a bare FTO-coated glass substrate was used as the reference). The bleaching condition (−0.7 V vs Ag/AgCl for 30 s) led to the transmittance enhancement of PVD-NNO, CSD-NNO, and ALD-NNO, all with a thickness of ∼50 nm, by 27, 24, and 11%, respectively. Note that the bleaching response of CSD-NNO/FTO is limited due to the high transmittance in the pristine state (67%). The inset of Figure 8h shows the transmittance modulation of a 100 nm thick CSD-NNO film grown on FTO, for which the pristine transmittance at 632.8 nm (55%) is comparable to that of 50 nm PVD-NNO/FTO (48%) or 50 nm ALD-NNO/FTO (61%). After bleaching (−0.7 V vs Ag/AgCl for 30 s), the transmittance of 100 nm CSD-NNO/FTO was increased by ∼40%. Further coloration treatment could modulate the transmittance of each sample back to the opaque state. This result is similar to the transmittance modulation trend observed in NNO films grown on LAO substrates. Optical images showing transmittance change upon bleaching in representative NNO/FTO glass samples can be found in Figure S2.

**Comparison of Film Performance between Synthesis Methods.** NNO thin films prepared by physical vapor deposition (PVD), chemical solution deposition (CSD), and atomic layer deposition (ALD) grew in an oriented manner on LAO substrates and were polycrystalline on FTO glass substrates (Figures 2 and 7). The films deposited in each method exhibited reversibly tunable optical transmittance due to proton (de-) intercalation (Figures 3, 6a–c, and 8g–i), with a proton diffusion coefficient of ∼1 × $10^{-7}$ $cm^2$ $s^{-1}$ (Figure 4d–f). Also, regardless of the deposition method, all films were stable in a pH 12 basic solution and could maintain more than 80% initial electroactivity after 400 cyclic voltammetry scans (Figures 5 and 8a–f). Due to the porous nature of chemical solution-deposited NNO films, they are more sensitive to bleaching and coloration treatments than dense NNO films deposited by PVD or ALD. For the same bleaching condition (−0.7 V vs Ag/AgCl for 30 s), CSD-NNO/LAO or CSD-NNO/FTO could increase transmittance by ∼40% (Table II) at 632.8 nm, while this value for PVD-NNO or ALD-NNO was much smaller (Table II). The transmittance of the bleached CSD-NNO (deposited on either LAO or FTO glass) film is higher than 90%. After bleaching, the coloration efficiency for CSD-NNO (47.9 $cm^2$ $C^{-1}$) is also much higher than that of PVD-NNO (17.9 $cm^2$ $C^{-1}$) and ALD-NNO (19.8 $cm^2$ $C^{-1}$) (Figure 6d–f). For application in smart windows, CSD-NNO films appear to show a greater degree of optical tunability compared to their denser counterparts synthesized by PVD or ALD. Similar enhancement of electrochromic performance due to microstructural aspects such as porosity has been noted in other oxide systems as well as in the literature.[7,14,49,51]

## CONCLUSIONS

We successfully synthesized and characterized a series of perovskite nickelate of $NdNiO_3$ (NNO) thin films on $LaAlO_3$- and FTO-coated glass substrates by PVD, CSD, and ALD methods. Their electrochromic properties in basic electrolytes (0.01 M KOH, pH = 12) were systematically studied. The films demonstrated tunable opacity at the visible wavelength via insertion/extraction of protons from aqueous electrolytes. Cycling experiments indicated that the material is stable in basic electrolytes. The high proton diffusion coefficient in NNO coupled with electrochemical stability is promising toward further exploration in smart window applications. Future directions include further optimization of microstructural features during deposition to enhance kinetics of chromic tuning. More specifically, some potential directions to further improve the electrochemical performances of NNO are as follows. The optimization of deposition parameters of chemical solution deposition such as solution viscosity control or adding pore-generating agents can be pursued, as it will help grow granular films for enhanced charge and mass transfer. Film patterning such as etching the film into high-density arrays could be expected to create a more active surface area, which would further improve the efficiency of bleaching or coloration. Chemical solution deposition is capable of depositing various nickelates including $NdNiO_3$, $SmNiO_3$, and even alloyed rare earth nickelates (e.g., $Sm_{1-x}Nd_xNiO_3$) with high quality as noted in the literature.[58] Considering that rare earth nickelates should behave similarly regarding the stability in basic electrolytes, it could be promising to study the effect of the chemical composition of the nickelates on electrochromic properties.

## ASSOCIATED CONTENT

### Supporting Information

The Supporting Information is available free of charge at https://pubs.acs.org/doi/10.1021/acsaelm.1c00030.

Atomic layer deposition process details, atomic layer deposition process optimization experiments, and optical images of NNO/FTO samples at pristine and bleached states (PDF)

## AUTHOR INFORMATION


### Corresponding Authors

**Qi Wang** − *School of Materials Engineering, Purdue University, West Lafayette, Indiana 47907, United States;* orcid.org/0000-0002-6314-7021; Email: wang3686@purdue.edu

**Shriram Ramanathan** − *School of Materials Engineering, Purdue University, West Lafayette, Indiana 47907, United States*; Email: shriram@purdue.edu

### Authors

**Yifei Sun** − *School of Materials Engineering, Purdue University, West Lafayette, Indiana 47907, United States;* orcid.org/0000-0002-2346-8402

**Tae Joon Park** − *School of Materials Engineering, Purdue University, West Lafayette, Indiana 47907, United States*

**Thomas Edward Gage** − *Center for Nanoscale Materials, Argonne National Laboratory, Lemont, Illinois 60439, United States*

**Zhen Zhang** − *School of Materials Engineering, Purdue University, West Lafayette, Indiana 47907, United States*

**Xuejing Wang** − *School of Materials Engineering, Purdue University, West Lafayette, Indiana 47907, United States*

**Di Zhang** − *School of Materials Engineering, Purdue University, West Lafayette, Indiana 47907, United States*

**Xing Sun** − *School of Materials Engineering, Purdue University, West Lafayette, Indiana 47907, United States*




https://doi.org/10.1021/acsaelm.1c00030
ACS Appl. Electron. Mater. XXXX, XXX, XXX−XXX

**Jiazhi He** − *Department of Chemistry, Purdue University, West Lafayette, Indiana 47907, United States*
**Hua Zhou** − *X-ray Science Division, Advanced Photon Source, Argonne National Laboratory, Lemont, Illinois 60439, United States;* orcid.org/0000-0001-9642-8674
**Daw Gen Lim** − *School of Materials Engineering, Purdue University, West Lafayette, Indiana 47907, United States*
**Chengzi Huang** − *School of Materials Engineering, Purdue University, West Lafayette, Indiana 47907, United States*
**Haoming Yu** − *School of Materials Engineering, Purdue University, West Lafayette, Indiana 47907, United States*
**Xuegang Chen** − *School of Materials Engineering, Purdue University, West Lafayette, Indiana 47907, United States*
**Haiyan Wang** − *School of Materials Engineering, Purdue University, West Lafayette, Indiana 47907, United States;* orcid.org/0000-0002-7397-1209
**Jianguo Mei** − *Department of Chemistry, Purdue University, West Lafayette, Indiana 47907, United States;* orcid.org/0000-0002-5743-2715
**Eric Deguns** − *Veeco ALD, Waltham, Massachusetts 02453, United States*

Complete contact information is available at: https://pubs.acs.org/10.1021/acsaelm.1c00030

### Author Contributions

#Y.S., Q.W., and T.J.P. contributed equally to this work.

### Notes

The authors declare no competing financial interest.

## ■ ACKNOWLEDGMENTS

X.W., D.Z., X.S., and H.W. acknowledge the funding support from the U.S. National Science Foundation for the microscopy work (DMR-2016453 and DMR-1809520). J.H. and J.M. acknowledge the support from Ambilight Inc. Y.S. and Q.W. were supported in part by AFOSR FA9550-19-1-0351 on the doping studies. H.Y. acknowledges the National Science Foundation (DMR-1904081) for support. The ALD and CSD equipment-related research were enabled through Purdue University startup grant. This work was performed, in part, at the Center for Nanoscale Materials, a U.S. Department of Energy Office of Science User Facility, and supported by the U.S. Department of Energy, Office of Science, under Contract No. DE-AC02-06CH11357. This research used resources of the Advanced Photon Source, a U.S. Department of Energy (DOE) Office of Science User Facility, operated for the DOE Office of Science by the Argonne National Laboratory under Contract No. DE-AC02-06CH11357. Extraordinary facility operations were supported, in part, by the DOE Office of Science through the National Virtual Biotechnology Laboratory, a consortium of DOE national laboratories focused on the response to COVID-19, with funding provided by the Coronavirus CARES Act.

## ■ ABBREVIATIONS

PVD-NNO:neodymium nickelate ($NdNiO_3$) thin film grown by physical vapor deposition (sputtering); CSD-NNO:neodymium nickelate ($NdNiO_3$) thin film grown by chemical solution deposition (spin-coating); ALD-NNO:neodymium nickelate ($NdNiO_3$) thin film grown by atomic layer deposition; LAO:lanthanum aluminate ($LaAlO_3$) substrate; FTO glass:fluorine-doped tin oxide-coated glass substrates

## ■ REFERENCES

(1) Cai, G. F.; Wang, J. X.; Lee, P. S. Next-Generation Multifunctional Electrochromic Devices. *Acc. Chem. Res.* **2016**, *49*, 1469−1476.
(2) Mortimer, R. J. Electrochromic materials. *Annu. Rev. Mater. Res.* **2011**, *41*, 241−268.
(3) Granqvist, C. G. Electrochromics for smart windows: Oxide-based thin films and devices. *Thin Solid Films* **2014**, *564*, 1−38.
(4) Yang, P.; Sun, P.; Du, L.; Liang, Z.; Xie, W.; Cai, X.; Huang, L.; Tan, S.; Mai, W. Quantitative Analysis of Charge Storage Process of Tungsten Oxide that Combines Pseudocapacitive and Electrochromic Properties. *J. Phys. Chem. C* **2015**, *119*, 16483−16489.
(5) Özer, N.; Chen, D. G.; Lampert, C. M. Preparation and properties of spin-coated Nb2O5 films by the sol-gel process for electrochromic applications. *Thin Solid Films* **1996**, *277*, 162−168.
(6) Wang, C.-M.; Lin, S.-Y.; Chen, Y.-C. Electrochromic properties of TiO2 thin films prepared by chemical solution deposition method. *J. Phys. Chem. Solids* **2008**, *69*, 451−455.
(7) Yuan, Y. F.; Xia, X. H.; Wu, J. B.; Chen, Y. B.; Yang, J. L.; Guo, S. Y. Enhanced electrochromic properties of ordered porous nickel oxide thin film prepared by self-assembled colloidal crystal template-assisted electrodeposition. *Electrochim. Acta* **2011**, *56*, 1208−1212.
(8) Jung, Y. W.; Lee, J.; Tak, Y. Electrochromic mechanism of IrO2 prepared by pulsed anodic electrodeposition. *Electrochem. Solid-State Lett.* **2004**, *7*, H5−H8.
(9) Wu, W.; Wang, M.; Ma, J.; Cao, Y.; Deng, Y. Electrochromic metal oxides: Recent progress and prospect. *Adv. Electron. Mater.* **2018**, *4*, No. 1800185.
(10) Niklasson, G. A.; Granqvist, C. G. Electrochromics for smart windows: thin films of tungsten oxide and nickel oxide, and devices based on these. *J. Mater. Chem.* **2007**, *17*, 127−156.
(11) Cong, S.; Tian, Y.; Li, Q.; Zhao, Z.; Geng, F. Single-crystalline tungsten oxide quantum dots for fast pseudocapacitor and electrochromic applications. *Adv. Mater.* **2014**, *26*, 4260−4267.
(12) Cai, G.; Cui, M.; Kumar, V.; Darmawan, P.; Wang, J.; Wang, X.; Eh, A. L.-S.; Qian, K.; Lee, P. S. Ultra-large optical modulation of electrochromic porous WO 3 film and the local monitoring of redox activity. *Chem. Sci.* **2016**, *7*, 1373−1382.
(13) Cheng, W.; He, J.; Dettelbach, K. E.; Johnson, N. J.; Sherbo, R. S.; Berlinguette, C. P. Photodeposited amorphous oxide films for electrochromic windows. *Chem* **2018**, *4*, 821−832.
(14) Wruck, D.; Rubin, M. Structure and electronic properties of electrochromic NiO films. *J. Electrochem. Soc.* **1993**, *140*, 1097−1104.
(15) Cai, G.; Wang, J.; Lee, P. S. Next-generation multifunctional electrochromic devices. *Acc. Chem. Res.* **2016**, *49*, 1469−1476.
(16) Zhao, C.; Chen, C.; Du, F.; Wang, J. Template synthesis of NiO ultrathin nanosheets using polystyrene nanospheres and their electrochromic properties. *RSC Adv.* **2015**, *5*, 38533−38537.
(17) Ma, D.; Shi, G.; Wang, H.; Zhang, Q.; Li, Y. Hierarchical NiO microflake films with high coloration efficiency, cyclic stability and low power consumption for applications in a complementary electrochromic device. *Nanoscale* **2013**, *5*, 4808−4815.
(18) Avendaño, E.; Azens, A.; Niklasson, G.; Granqvist, C. Proton Diffusion and Electrochromism in Hydrated NiO y and Ni1− x V x O y Thin Films. *J. Electrochem. Soc.* **2005**, *152*, F203−F212.
(19) Gavrilyuk, A. I. Photochromism in WO3 thin films. *Electrochim. Acta* **1999**, *44*, 3027−3037.
(20) Novojilov, M.; Gorbenko, O. Y.; Graboy, I.; Kaul, A.; Zandbergen, H.; Babushkina, N.; Belova, L. Perovskite rare-earth nickelates in the thin-film epitaxial state. *Appl. Phys. Lett.* **2000**, *76*, 2041−2043.
(21) Li, Z.; Zhou, Y.; Qi, H.; Pan, Q.; Zhang, Z.; Shi, N. N.; Lu, M.; Stein, A.; Li, C. Y.; Ramanathan, S.; Yu, N. Correlated Perovskites as a New Platform for Super-Broadband-Tunable Photonics. *Adv. Mater.* **2016**, *28*, 9117−9125.
(22) Khomskii, D. Role of orbitals in the physics of correlated electron systems. *Phys. Scr.* **2005**, *72*, CC8.
(23) Catalan, G. Progress in perovskite nickelate research. *Phase Transitions* **2008**, *81*, 729−749.

(24) Oh, C.; Jo, M.; Son, J. All-Solid-State Synaptic Transistors with High-Temperature Stability Using Proton Pump Gating of Strongly Correlated Materials. *ACS Appl. Mater. Interfaces* **2019**, *11*, 15733−15740.
(25) Wang, L.; Stoerzinger, K. A.; Chang, L.; Zhao, J.; Li, Y.; Tang, C. S.; Yin, X.; Bowden, M. E.; Yang, Z.; Guo, H.; et al. Tuning Bifunctional Oxygen Electrocatalysts by Changing the A-Site Rare-Earth Element in Perovskite Nickelates. *Adv. Funct. Mater.* **2018**, *28*, No. 1803712.
(26) Chen, J.; Mao, W.; Gao, L.; Yan, F.; Yajima, T.; Chen, N.; Chen, Z.; Dong, H.; Ge, B.; Zhang, P.; Cao, X.; Wilde, M.; Jiang, Y.; Terai, T.; Shi, J. Electron-Doping Mottronics in Strongly Correlated Perovskite. *Adv. Mater.* **2020**, *32*, No. 1905060.
(27) Chen, J.; Mao, W.; Ge, B.; Wang, J.; Ke, X.; Wang, V.; Wang, Y.; Döbeli, M.; Geng, W.; Matsuzaki, H.; Shi, J.; Jiang, Y. Revealing the role of lattice distortions in the hydrogen-induced metal-insulator transition of SmNiO3. *Nat. Commun.* **2019**, *10*, No. 694.
(28) Guo, Q.; Farokhipoor, S.; Magen, C.; Rivadulla, F.; Noheda, B. Tunable resistivity exponents in the metallic phase of epitaxial nickelates. *Nat. Commun.* **2020**, *11*, No. 2949.
(29) Wang, L.; Stoerzinger, K. A.; Chang, L.; Yin, X.; Li, Y.; Tang, C. S.; Jia, E.; Bowden, M. E.; Yang, Z.; Abdelsamie, A.; You, L.; Guo, R.; Chen, J.; Rusydi, A.; Wang, J.; Chambers, S. A.; Du, Y. Strain Effect on Oxygen Evolution Reaction Activity of Epitaxial NdNiO3 Thin Films. *ACS Appl. Mater. Interfaces* **2019**, *11*, 12941−12947.
(30) Oh, C.; Heo, S.; Jang, H. M.; Son, J. Correlated memory resistor in epitaxial NdNiO3 heterostructures with asymmetrical proton concentration. *Appl. Phys. Lett.* **2016**, *108*, No. 122106.
(31) Kawamoto, D.; Hattori, A. N.; Yamamoto, M.; Tan, X. L.; Hattori, K.; Daimon, H.; Tanaka, H. Correlation between Ni Valence and Resistance Modulation on a SmNiO3 Chemical Transistor. *ACS Appl. Electron. Mater.* **2019**, *1*, 82−87.
(32) Zhang, H. T.; Park, T. J.; Zaluzhnyy, I. A.; Wang, Q.; Wadekar, S. N.; Manna, S.; Andrawis, R.; Sprau, P. O.; Sun, Y.; Zhang, Z.; Huang, C.; Zhou, H.; Zhang, Z.; Narayanan, B.; Srinivasan, G.; Hua, N.; Nazaretski, E.; Huang, X.; Yan, H.; Ge, M.; Chu, Y. S.; Cherukara, M. J.; Holt, M. V.; Krishnamurthy, M.; Shpyrko, O. G.; Sankaranarayanan, S.; Frano, A.; Roy, K.; Ramanathan, S. Perovskite neural trees. *Nat. Commun.* **2020**, *11*, No. 2245.
(33) Bard, A. J.; Faulkner, L. R.; Leddy, J.; Zoski, C. G. *Electrochemical Methods: Fundamentals and Applications*; Wiley: New York, 1980; Vol. 2.
(34) Guidelli, R.; Compton, R. G.; Feliu, J. M.; Gileadi, E.; Lipkowski, J.; Schmickler, W.; Trasatti, S. Defining the transfer coefficient in electrochemistry: An assessment (IUPAC Technical Report). *Pure Appl. Chem.* **2014**, *86*, 245−258.
(35) Preziosi, D.; Sander, A.; Barthélémy, A.; Bibes, M. Reproducibility and off-stoichiometry issues in nickelate thin films grown by pulsed laser deposition. *AIP Adv.* **2017**, *7*, No. 015210.
(36) Kumar, Y.; Choudhary, R. J.; Kumar, R. Strain controlled systematic variation of metal-insulator transition in epitaxial NdNiO3 thin films. *J. Appl. Phys.* **2012**, *112*, No. 073718.
(37) Dalavi, D. S.; Devan, R. S.; Patil, R. S.; Ma, Y.-R.; Patil, P. S. Electrochromic performance of sol−gel deposited NiO thin film. *Mater. Lett.* **2013**, *90*, 60−63.
(38) Pontes, D. S. L.; Pontes, F. M.; Pereira-da-Silva, M. A.; Berengue, O. M.; Chiquito, A. J.; Longo, E. Structural and electrical properties of LaNiO3 thin films grown on (100) and (001) oriented SrLaAlO4 substrates by chemical solution deposition method. *Ceram. Int.* **2013**, *39*, 8025−8034.
(39) Schwartz, R. W.; Schneller, T.; Waser, R. Chemical solution deposition of electronic oxide films. *C. R. Chim.* **2004**, *7*, 433−461.
(40) Zhu, X.; Tang, X.; Wang, B.; Fu, Y.; Dai, J.; Song, W.; Yang, Z.; Zhu, X.; Chen, L.; Sun, Y. Epitaxial Growth by Chemical Solution Deposition of (110) NdNiO3−$\delta$Films with a Sharp Metal−Insulator Transition Annealed under Ambient Oxygen. *Cryst. Growth Des.* **2010**, *10*, 4682−4685.
(41) Zaghrioui, M.; Bulou, A.; Lacorre, P.; Laffez, P. Electron diffraction and Raman scattering evidence of a symmetry breaking at the metal-insulator transition of NdNiO3. *Phys. Rev. B* **2001**, *64*, No. 081102.
(42) Girardot, C.; Kreisel, J.; Pignard, S.; Caillault, N.; Weiss, F. Raman scattering investigation across the magnetic and metal-insulator transition in rare earth nickelate RNiO3 (R = Sm, Nd) thin films. *Phys. Rev. B* **2008**, *78*, No. 104101.
(43) Randin, J. P.; Viennet, R. Proton Diffusion in Tungsten Trioxide Thin Films. *J. Electrochem. Soc.* **1982**, *129*, 2349−2354.
(44) Haranahalli, A.; Holloway, P. The influence of metal overlayers on electrochromic behavior of WO3 films. *J. Electron. Mater.* **1981**, *10*, 141−172.
(45) Opallo, M.; Prokopowicz, A. Low temperature study of nickel hydroxide electrode in frozen electrolyte. *Electrochem. Commun.* **2003**, *5*, 737−740.
(46) Patil, S. J.; Patil, B. H.; Bulakhe, R. N.; Lokhande, C. D. Electrochemical performance of a portable asymmetric supercapacitor device based on cinnamon-like La2Te3prepared by a chemical synthesis route. *RSC Adv.* **2014**, *4*, 56332−56341.
(47) Silva, L. S. R.; López-Suárez, F. E.; Perez-Cadenas, M.; Santos, S. F.; da Costa, L. P.; Eguiluz, K. I. B.; Salazar-Banda, G. R. Synthesis and characterization of highly active Pb x @Pt y/C core-shell nanoparticles toward glycerol electrooxidation. *Appl. Catal., B* **2016**, *198*, 38−48.
(48) Steven, J. T.; Golovko, V. B.; Johannessen, B.; Marshall, A. T. Electrochemical stability of carbon-supported gold nanoparticles in acidic electrolyte during cyclic voltammetry. *Electrochim. Acta* **2016**, *187*, 593−604.
(49) Xia, X.; Tu, J.; Zhang, J.; Wang, X.; Zhang, W.; Huang, H. Morphology effect on the electrochromic and electrochemical performances of NiO thin films. *Electrochim. Acta* **2008**, *53*, 5721−5724.
(50) Kitao, M.; Izawa, K.; Urabe, K.; Komatsu, T.; Kuwano, S.; Yamada, S. Preparation and electrochromic properties of RF-sputtered NiOx films prepared in Ar/O2/H2 atmosphere. *Jpn. J. Appl. Phys.* **1994**, *33*, 6656.
(51) Ren, Y.; Zhou, X.; Zhang, H.; Lei, L.; Zhao, G. Preparation of a porous NiO array-patterned film and its enhanced electrochromic performance. *J. Mater. Chem. C* **2018**, *6*, 4952−4958.
(52) Najafi-Ashtiani, H.; Bahari, A.; Gholipour, S. Investigation of coloration efficiency for tungsten oxide−silver nanocomposite thin films with different surface morphologies. *J. Mater. Sci.: Mater. Electron.* **2018**, *29*, 5820−5829.
(53) Heo, S.; Dahlman, C. J.; Staller, C. M.; Jiang, T.; Dolocan, A.; Korgel, B. A.; Milliron, D. J. Enhanced Coloration Efficiency of Electrochromic Tungsten Oxide Nanorods by Site Selective Occupation of Sodium Ions. *Nano Lett.* **2020**, *20*, 2072−2079.
(54) Chen, Y.; Wang, Y.; Sun, P.; Yang, P.; Du, L.; Mai, W. Nickel oxide nanoflake-based bifunctional glass electrodes with superior cyclic stability for energy storage and electrochromic applications. *J. Mater. Chem. A* **2015**, *3*, 20614−20618.
(55) Koo, B.-R.; Ahn, H.-J. Fast-switching electrochromic properties of mesoporous WO3 films with oxygen vacancy defects. *Nanoscale* **2017**, *9*, 17788−17793.
(56) Wang, W.-q.; Wang, X.-l.; Xia, X.-h.; Yao, Z.-j.; Zhong, Y.; Tu, J.-p. Enhanced electrochromic and energy storage performance in mesoporous WO3 film and its application in a bi-functional smart window. *Nanoscale* **2018**, *10*, 8162−8169.
(57) Alonso, J. A.; Demazeau, G.; Largeteau, A.; Kurowski, D.; Hoffmann, R.-D.; Pöttgen, R. Crystal Structure of NdNiO3 at 123 and 292 K. *Z. Naturforsch. B* **2006**, *61*, 346−349.
(58) Chen, J.; Hu, H.; Wang, J.; Yajima, T.; Ge, B.; Ke, X.; Dong, H.; Jiang, Y.; Chen, N. Overcoming synthetic metastabilities and revealing metal-to-insulator transition & thermistor bi-functionalities for d-band correlation perovskite nickelates. *Mater. Horiz.* **2019**, *6*, 788−795.
(59) Faughnan, B. W.; Crandall, R. S. Electrochromic Displays Based on WO3. In *Display Devices*; Pankove, J. I., Ed.; Springer: Berlin, 1980; pp 181−211.


https://doi.org/10.1021/acsaelm.1c00030
*ACS Appl. Electron. Mater.* XXXX, XXX, XXX−XXX

(60) Kumar, V.; Wang, X.; Lee, P. S. Formation of hexagonal-molybdenum trioxide (h-MoO3) nanostructures and their pseudocapacitive behavior. *Nanoscale* **2015**, *7*, 11777−11786.
(61) Hanzu, I.; Djenizian, T.; Knauth, P. Electrical and Point Defect Properties of TiO2 Nanotubes Fabricated by Electrochemical Anodization. *J. Phys. Chem. C* **2011**, *115*, 5989−5996.


https://doi.org/10.1021/acsaelm.1c00030
*ACS Appl. Electron. Mater.* XXXX, XXX, XXX−XXX